JACS
JOURNAL OF THE AMERICAN CHEMICAL SOCIETY
Communication
pubs.acs.org/JACS

# Intrinsic White-Light Emission from Layered Hybrid Perovskites

Emma R. Dohner,[†] Adam Jaffe,[†] Liam R. Bradshaw,[§] and Hemamala I. Karunadasa*,[†]

[†]Department of Chemistry, Stanford University, Stanford, California 94305, United States
[§]Department of Chemistry, University of Washington, Seattle, Washington 98195, United States

Supporting Information

**ABSTRACT:** We report on the second family of layered perovskite white-light emitters with improved photoluminescence quantum efficiencies (PLQEs). Upon near-ultraviolet excitation, two new Pb−Cl and Pb−Br perovskites emit broadband "cold" and "warm" white light, respectively, with high color rendition. Emission from large, single crystals indicates an origin from the bulk material and not surface defect sites. The Pb−Br perovskite has a PLQE of 9%, which is undiminished after 3 months of continuous irradiation. Our mechanistic studies indicate that the emission has contributions from strong electron−phonon coupling in a deformable lattice and from a distribution of intrinsic trap states. These hybrids provide a tunable platform for combining the facile processability of organic materials with the structural definition of crystalline, inorganic solids.

Recently, we described white-light emission upon near-ultraviolet excitation from the family of layered hybrid perovskites (*N*-MEDA)[$PbBr_{4-x}Cl_x$] (*N*-MEDA = $N^1$-methylethane-1,2-diammonium, $x$ = 0−1.2).[1] Broadband emission from these materials displayed high color rendition, tunable chromaticity coordinates, and undiminished activity under continuous irradiation for a week. However, the photoluminescence quantum efficiencies (PLQEs) were 0.5−1.5%. Here, we report on a new family of white-light-emitting perovskites with PLQEs of up to 9%, which show stable emission over at least 3 months of continuous irradiation. Broadband white-light emission arises from Pb−Cl and Pb−Br inorganic sheets that can be derived from the (100) and (110) crystallographic planes of the three-dimensional perovskite structure, respectively. Similar emission spectra and quantum yields from cm-scale single crystals (Figure 1) as well as $\mu$m-scale particles indicate an origin from the bulk structure and not surface defect sites. Variable-temperature photoluminescence (PL) studies on the Pb−Br perovskite support coupling between photogenerated electrons/holes and lattice distortions. Assuming a harmonic lattice and linear electron−phonon coupling, we estimate the effective frequency of lattice vibrations coupled to the electronic transition to be in the region of typical Pb−Br bond frequencies. We also discuss contributions to the emission bandwidth from inhomogeneous broadening due to a distribution of emissive trap states and probe the nature of these defects.

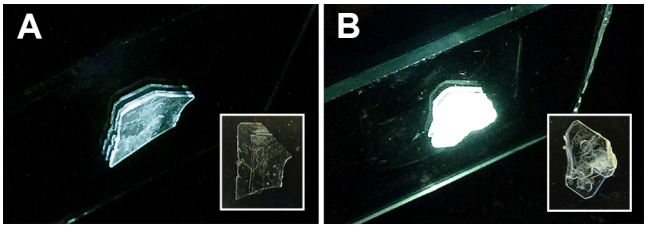


**Figure 1.** Photographs showing photoluminescence from (A) a 1 × 0.5 × 0.1 cm single crystal of **1**-Cl and (B) a 1 × 0.4 × 0.1 cm single crystal of **2**-Br, under 310 and 365 nm irradiation, respectively. Insets show photographs of the crystals in ambient light.

Combining $PbX_2$ and $(EDBE)X_2$ (EDBE = 2,2′-(ethylenedioxy)bis(ethylammonium); X = Cl, Br, and I) in corresponding aqueous HX solutions afforded the (EDBE)-[$PbX_4$] (X = Cl (**1**-Cl), Br (**2**-Br), and I (**3**-I)) family of layered perovskites (Figure 2).[2] The structure of **1**-Cl contains (100) inorganic sheets with pronounced distortion from octahedral geometry around the $Pb^{II}$ centers. The other members, **2**-Br and **3**-I, contain (110) inorganic sheets with a more regular octahedral coordination environment for the metal (Supporting Information, Tables S2 and S3). In **2**-Br and **3**-I, hydrogen bonds between terminal ammonium groups and oxygens in adjacent organic molecules enforce a paired configuration for EDBE cations, which likely stabilize the (110) structure (Figure 2).

Absorption spectra of these materials are similar to those of other two-dimensional lead−halide perovskites.[3] The dielectric mismatch between organic and inorganic layers leads to strongly bound excitons,[4] reflected in the sharp excitonic absorption bands at 351, 371, and 470 nm for **1**-Cl, **2**-Br, and **3**-I, respectively (Figure 3A−C). Upon excitation at 310 nm, **1**-Cl shows a broad emission spanning the entire visible spectrum, with a maximum at 538 nm and a full width at half-maximum (fwhm) of 208 nm (0.95 eV). The emission also features a less intense but well-defined shoulder at 358 nm. Similarly, upon 365 nm excitation, **2**-Br shows a broad emission with a maximum at 573 nm and a fwhm of 215 nm (0.80 eV). Here also, a higher-energy shoulder at 410 nm is evident but less defined. In contrast to the Cl and Br analogues, **3**-I displays a sharper green emission at 515 nm with a fwhm of 70 nm (0.32 eV) and a significantly smaller Stokes shift of 45 nm when excited at 400 nm. We calculated[5] the PLQEs of **1**-Cl and **2**-Br to be 2% and 9%, respectively. The latter constitutes an 18-fold improvement over the PLQE of our first-generation material,

**Received:** July 13, 2014

   dx.doi.org/10.1021/ja507086b | J. Am. Chem. Soc. XXXX, XXX, XXX−XXX

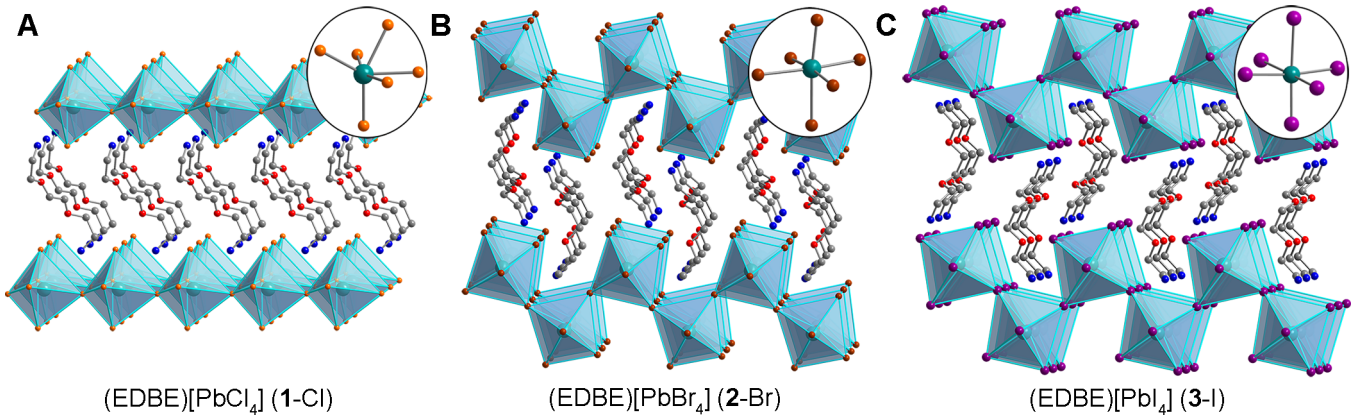


**Figure 2.** X-ray structures of (EDBE)[$PbX_4$]: (A) X = Cl (**1**-Cl), (B) X = Br (**2**-Br), and (C) X = I (**3**-I) (EDBE = 2,2′-(ethylenedioxy)bis(ethylammonium)). Turquoise, purple, brown, orange, red, blue, and gray spheres represent Pb, I, Br, Cl, O, N, and C atoms, respectively. H atoms are omitted for clarity. Insets show lead coordination environments.

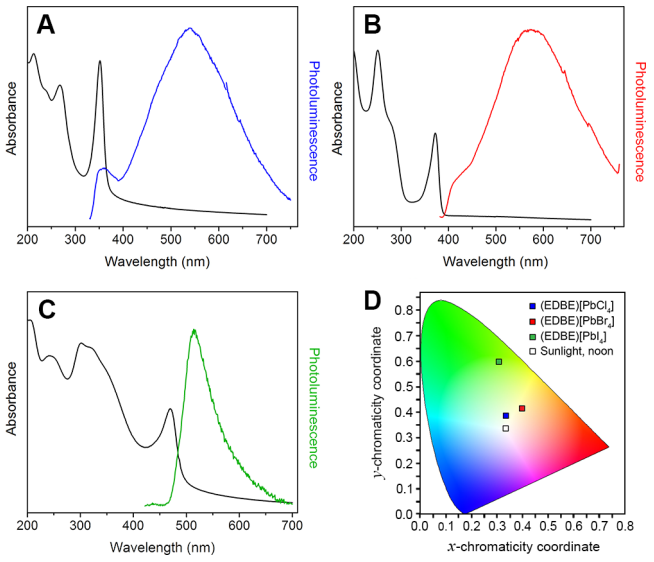


**Figure 3.** Absorption (black) and emission (colored) spectra for (A) **1**-Cl, $\lambda_{ex}$ = 310 nm; (B) **2**-Br, $\lambda_{ex}$ = 365 nm; and (C) **3**-I, $\lambda_{ex}$ = 400 nm. (D) Chromaticity coordinates of the emissions.

(*N*-MEDA)[$PbBr_4$]. The narrow emission of **3**-I has a PLQE of less than 0.5%.

Emission from **2**-Br has CIE chromaticity coordinates[6] of (0.39, 0.42), with a larger contribution from the red region of the spectrum compared to pure white light, which has chromaticity coordinates of (0.33, 0.33) (Figure 3D). This gives the emission from **2**-Br a correlated color temperature (CCT) of 3990 K, corresponding to "warm" white light that is ideal for indoor illumination.[6] The broad emission also leads to a high color-rendering index (CRI) of 84. CRI values quantify how accurately illuminated colors are reproduced compared with a blackbody light source; indoor lighting applications typically require values above 80.[6b] Emission from **2**-Br under continuous illumination is also remarkably stable. A crystalline sample, enclosed in a vacuum-sealed quartz ampule, showed no change in emission color or intensity during 3 months of continuous irradiation with a 4-W (720 $\mu W/cm^2$), 365 nm lamp. Emission from **1**-Cl has CIE coordinates of (0.33, 0.39), a CCT of 5509 that affords "cold" white light, and a CRI of 81 (Figure 3D).

Before studying the emission mechanism, we sought to establish that white-light emission was a bulk effect and not a result of surface defects. In materials such as CdSe quantum dots, white-light emission has been attributed to mid-bandgap states arising from deep traps at surface sites. This emission shows a strong dependence on particle size and is readily quenched by particle aggregation.[7] In contrast, we observe similar emission profiles and PLQEs from cm-sized single crystals and $\mu$m-sized particles of **1**-Cl and **2**-Br (Figure 1 and Supporting Information, Figure S8), indicating that defects at the crystal surface are not the origin of the emission. Due to its higher PLQE, we conducted subsequent mechanistic studies on **2**-Br. Solution-state assembly affords the mixed-halide series (EDBE)[$PbBr_{4-x}Cl_x$] ($x$ = 0−1.8; determined through inductively coupled plasma mass spectrometry). For these values of $x$, (EDBE)[$PbBr_{4-x}Cl_x$] is isostructural with **2**-Br and shows a decrease in lattice spacings upon substitution of chloride for bromide (Figure S9). Reflectance measurements show a blue-shift in both the exciton absorption and bandgap energies with increasing chloride content (Figure S10). This is consistent with stabilization of the predominantly halide-based valence band due to the greater electronegativity of Cl compared to Br.[8] Upon increasing chloride substitution, the (EDBE)[$PbBr_{4-x}Cl_x$] family displays a gradual decrease in overall emission intensity, accompanied by a blue-shift in the higher-energy shoulder when irradiated at the corresponding exciton absorption energy. In contrast, the position and band shape of the broad emission remain constant (Figure S10), indicating that the excited state involved in the broad emission does not possess significant chloride character. For example, transition energies of excited electrons in the lead-based conduction band to bromide-based hole traps should be insensitive to chloride content. Reports on excited states of $PbBr_2$[9] and one-dimensional Pb−Br structures[10] describe holes in similar Br-based trap states and electrons trapped at Pb sites. Iodide substitution in (EDBE)[$PbBr_{4-x}I_x$] ($x$ = 0−3.9) leads to a red-shift of the higher-energy shoulder, while the position of the broad emission remains unchanged (Figure S12). Here, the emission intensity decreases abruptly upon halide substitution. At $x$ = 3.9, the broad emission disappears and the higher-energy shoulder matches the emission spectrum of **3**-I, suggesting a similar origin for the emission of **3**-I and the higher-energy shoulder of **2**-Br. This shoulder accompanies the broad emission in **2**-Br at temperatures above 150 K, with the


dx.doi.org/10.1021/ja507086b | J. Am. Chem. Soc. XXXX, XXX, XXX−XXX

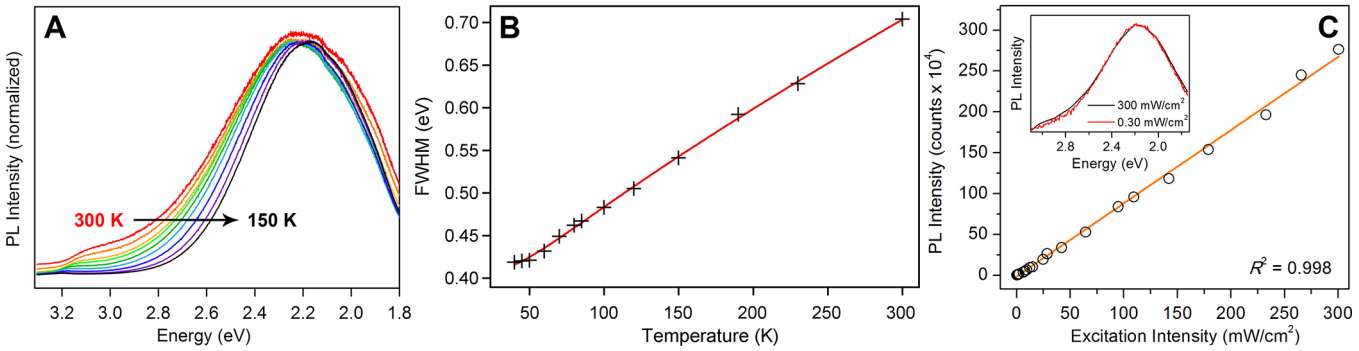


**Figure 4.** (A) Temperature dependence of the emission from **2**-Br (spectra are normalized to the maximum at ca. 2.2 eV and offset for clarity). (B) Temperature dependence of the main emission bandwidth in **2**-Br (black symbols) and a fit to a model that includes contributions from vibronic coupling and inhomogeneous broadening due to defect sites (red line). (C) Dependence of emission intensity at 565 nm in **2**-Br on excitation intensity (0.295−300 mW/cm$^2$; black symbols) at 300 K and a linear fit (orange line; $\lambda_{ex}$ = 355 nm) (inset shows emission profiles at high and low excitation intensities).

relative intensity of the shoulder increasing at higher temperatures (Figure 4A). Both the shoulder and the broad emission are excited through the same absorption features at 384 and 330 nm and have the same lifetime of 14(1) ns, indicating fast thermal equilibrium between their excited states (Figures S14 and S15).

Our initial mechanistic studies indicate that white-light emission from **2**-Br likely has contributions from both distorted excited states due to strong electron−phonon coupling in a deformable lattice as well as inhomogeneous broadening resulting from a distribution of trap states. Strong coupling of excited electrons/holes to lattice deformations can lead to a broad emission with a pronounced Stokes shift due to stabilized, distorted electronic states (Figure S16).[11] Consistent with electron−lattice coupling, the broad emission becomes more intense and narrower with decreasing temperature. Accordingly, the emission's PLQE increases with decreasing temperature and reaches 85(1)% at 105 K (Figure S18). Between 300 and 50 K, the major part of the broad emission is fit well by a Gaussian distribution function (Figure S19). Assuming linear electron−phonon coupling and harmonic lattice vibrations, the temperature dependence of the fwhm of this Gaussian emission allows us to estimate the effective frequency of vibrational modes coupled to the electronic transition using the following model:[12]

$$\Gamma(T) = \Gamma_0 + \Gamma_{\text{phonon}}(e^{E_{\text{LO}}/k_{\text{B}}T} - 1)^{-1} + \Gamma_{\text{inhomo}}\, e^{-E_{\text{b}}/k_{\text{B}}T}$$

Here, $\Gamma_0$ represents the emission fwhm at $T$ = 0 K, $E_{\text{LO}}$ is the energy of the longitudinal optical phonon mode coupled to the electronic transition, and $E_{\text{b}}$ represents the average binding energy of emissive defect states. The constants $\Gamma_{\text{phonon}}$ and $\Gamma_{\text{inhomo}}$ give the relative contributions of electron−phonon coupling and inhomogeneous broadening to the emission line width. A fit to the data (Figure 4B) gives $E_{\text{LO}}$ = 12(1) meV, $E_{\text{b}}$ = 11(2) meV, and $\Gamma_0$, $\Gamma_{\text{phonon}}$, and $\Gamma_{\text{inhomo}}$ = 410(5), 130(7), and 120(5) meV, respectively. This $E_{\text{LO}}$ corresponds to a frequency of 97 cm$^{-1}$, which lies in the range of Pb−Br stretching frequencies in **2**-Br (Figure S20B).

To probe the identity of emissive trap states in **2**-Br, we attempted to change the defect concentration in the material and assess if the emission could be enhanced or suppressed. Ball-milled powders of **2**-Br were pressed into pellets at 10 000 psi and annealed at 150 °C for 24 h. Powder X-ray diffraction patterns showed an increase in crystallinity in the annealed samples, but emission spectra obtained before and after annealing were within experimental error (Figure S22). Microcrystalline powders precipitated from solution at −25, 0, and 28 °C also showed the same emission (Figure S23), indicating that differences in crystallization rates at these temperatures do not affect the emission. We then studied the emission's dependence on excitation intensity. If the emission arises from permanent defects, we would expect PL saturation as these traps become filled.[13] PL intensity increases linearly with excitation power density from 0.295 to 300 mW/cm$^2$ at 300 K (Figure 4C), with no signs of PL saturation. Although material degradation precluded the use of higher excitation intensities, this linear behavior suggests that emission does not arise from permanent material defects (see Supporting Information for details). We also see no change in emission band shape throughout this experiment (Figure 4C inset), indicating that different emissive defect sites are not accessed at different excitation intensities. As an alternative to permanent defects, photogenerated electrons/holes can couple to lattice distortions and be stabilized as "self-trapped" carriers[14] that act as "excited-state defects". Although further studies are required to confirm this mechanism, the linear power dependence and the insensitivity of emission band shape to excitation intensity are consistent with emission from such photogenerated trap states.[15] Emission from $PbBr_2$[9] and Pb−Br[10] chain structures has been attributed to such self-trapped states. For example, upon irradiation of $PbBr_2$, adjacent $Br^-$ sites trap holes as $Br_2^-$ dimers.[9]

The electronic structures of layered metal−halide perovskites show narrow bands conducive for charge localization.[8a] Due to its low dielectric constant, the organic layer provides poor shielding between photogenerated electrons and holes in the inorganic layer, resulting in more strongly bound excitons compared to three-dimensional perovskites.[4a] The emission's dependence on temperature and excitation power density is consistent with tightly bound excitons that are further stabilized as self-trapped excitons or as separately trapped electrons/holes through coupling to lattice distortions. Furthermore, we have so far observed white-light emission only from perovskites with (110) sheets and distorted (100) sheets, suggesting that the emission is influenced by the bulk crystal structure.

Single phosphors typically produce light with poor color rendition because of their narrow emission widths, while devices with multiple phosphors suffer from efficiency losses due to self-absorption as well as changes in the emission color


dx.doi.org/10.1021/ja507086b | J. Am. Chem. Soc. XXXX, XXX, XXX−XXX

as individual phosphors degrade at different rates.[6] Therefore, achieving broadband white light from a single phosphor is a major goal in solid-state lighting technology. This new class of single-source, broadband white-light emitters has many promising attributes as phosphors, although the PLQEs must be increased for lighting applications. Furthermore, these organic−inorganic hybrids can be processed using solution-state methods used for organic phosphors, which may enable applications requiring inexpensive, large-area coatings. Intrinsic white-light emission from bulk materials is rare; other examples of similar emitters include the $Cd_{2-x}Zn_xE_2$(alkylamine) (E = S, Se, and Te) compounds.[16] Most inorganic white-light phosphors require emissive dopants (e.g., $Eu^{3+}$, $Ce^{3+}$)[6] or surface sites (e.g., quantum dots).[7a] In contrast, our initial mechanistic studies indicate that the unusually broad emission in **2**-Br is an intrinsic bulk property, which may be more amenable to synthetic design.

## ■ ASSOCIATED CONTENT

### Supporting Information

Experimental details, optical spectra, and crystallographic data. This material is available free of charge via the Internet at http://pubs.acs.org. CIFs for (EDBE)[$PbBr_4$], (EDBE)[$PbI_4$], and (EDBE)[$PbCl_4$] have been deposited in the Cambridge Crystallographic Data Centre under deposition numbers CCDC 993477−9934779, respectively.

## ■ AUTHOR INFORMATION


### Corresponding Author

hemamala@stanford.edu


### Notes

The authors declare no competing financial interest.

## ■ ACKNOWLEDGMENTS

We thank Stanford Undergraduate Advising and Research for support of E.R.D., the Satre Family for support of A.J. through the Stanford Interdisciplinary Graduate Fellowship, and the Precourt Institute for Energy for research funds. X-ray diffraction studies were performed at the Stanford Nano-characterization Laboratory. We thank Profs. D. R. Gamelin and E. I. Solomon for valuable discussions and Dr. E. T. Hoke and D. J. Slotcavage for experimental assistance.

## ■ REFERENCES


(1) Dohner, E. R.; Hoke, E. T.; Karunadasa, H. I. *J. Am. Chem. Soc.* **2014**, *136*, 1718.

(2) Crystal structure refinement parameters: For **1**-Cl, $C_6H_{18}O_2N_2PbCl_4$, $T$ = 100(2) K, $C2$, $Z$ = 2, $a$ = 7.7316(10) Å, $b$ = 7.5418(10) Å, $c$ = 13.2928(18) Å, $\beta$ = 102.481(4)°, $V$ = 756.79(17) Å$^3$, $R_1$ = 0.0285, w$R_2$ = 0.0786. For **2**-Br, $C_6H_{18}O_2N_2PbBr_4$, $T$ = 100(2) K, $P2_1/c$, $Z$ = 4, $a$ = 6.0917(3) Å, $b$ = 28.7804(14) Å, $c$ = 8.8860(4) Å, $\beta$ = 91.852(2)°, $V$ = 1557.09(13) Å$^3$, $R_1$ = 0.0234, w$R_2$ = 0.0623. For **3**-I, $C_6H_{18}O_2N_2PbI_4$, $T$ = 100(2) K, $P2_1/c$, $Z$ = 4, $a$ = 6.4940(5) Å, $b$ = 29.461(2) Å, $c$ = 9.2666(7) Å, $\beta$ = 91.777(2)°, $V$ = 1772.0(2) Å$^3$, $R_1$ = 0.0163, w$R_2$ = 0.0415.

(3) (a) Ishihara, T. In *Optical Properties of Low-Dimensional Materials*; Ogawa, T., Kanemitsu, Y., Eds.; World Scientific Publishing Co.: Singapore, 1995; p 288. (b) Mitzi, D. B. *Prog. Inorg. Chem.* **1999**, *48*, 1.

(4) (a) Muljarov, E. A.; Tikhodeev, S. G.; Gippius, N. A.; Ishihara, T. *Phys. Rev. B* **1995**, *51*, 14370. (b) Kitazawa, N.; Aono, M.; Watanabe, Y. *Thin Solid Films* **2010**, *518*, 3199.

(5) de Mello, J. C.; Wittmann, H. F.; Friend, R. H. *Adv. Mater.* **1997**, *9*, 230.

(6) (a) Ye, S.; Xiao, F.; Pan, Y. X.; Ma, Y. Y.; Zhang, Q. Y. *Mater. Sci. Eng., R* **2010**, *71*, 1. (b) Silver, J.; Withnall, R. In *Luminescent Materials*; Kitai, A., Ed.; John Wiley & Sons: Chicester, 2008; p 75.

(7) (a) Bowers, M. J.; McBride, J. R.; Rosenthal, S. J. *J. Am. Chem. Soc.* **2005**, *127*, 15378. (b) Noh, M.; Kim, T.; Lee, H.; Kim, C.-K.; Joo, S.-W.; Lee, K. *Colloids Surf., A* **2010**, *359*, 39.

(8) (a) Umebayashi, T.; Asai, K.; Kondo, T.; Nakao, A. *Phys. Rev. B* **2003**, *67*, 155405. (b) Ishihara, T.; Hirasawa, M.; Goto, T. *Jpn. J. Appl. Phys.* **1995**, *34S1*, 71.

(9) Iwanaga, M.; Azuma, J.; Shirai, M.; Tanaka, K.; Hayashi, T. *Phys. Rev. B* **2002**, *65*, 214306.

(10) Azuma, J.; Tanaka, K.; Kan'no, K.-i. *J. Phys. Soc. Jpn.* **2002**, *71*, 971.

(11) Solomon, E. I. *Comments Inorg. Chem.* **1984**, *3*, 300.

(12) (a) Fonoberov, V. A.; Alim, K. A.; Balandin, A. A.; Xiu, F.; Liu, J. *Phys. Rev. B* **2006**, *73*, 165317. (b) Lee, J.; Koteles, E. S.; Vassell, M. O. *Phys. Rev. B* **1986**, *33*, 5512.

(13) (a) Tongay, S.; Suh, J.; Ataca, C.; Fan, W.; Luce, A.; Kang, J. S.; Liu, J.; Ko, C.; Raghunathanan, R.; Zhou, J.; Ogletree, F.; Li, J.; Grossman, J. C.; Wu, J. *Sci. Rep.* **2013**, *3*, 2657. (b) Schmidt, T.; Lischka, K.; Zulehner, W. *Phys. Rev. B* **1992**, *45*, 8989.

(14) Toyozawa, Y. *Prog. Theor. Phys.* **1961**, *26*, 29.

(15) Netzel, C.; Hoffmann, V.; Wernicke, T.; Knauer, A.; Weyers, M.; Kneissl, M.; Szabo, N. *J. Appl. Phys.* **2010**, *107*, 033510.

(16) (a) Ki, W.; Li, J. *J. Am. Chem. Soc.* **2008**, *130*, 8114. (b) Roushan, M.; Zhang, X.; Li, J. *Angew. Chem., Int. Ed.* **2012**, *51*, 436.